

# Recognition of Cognate Transfer RNA by the 30S Ribosomal Subunit

James M. Ogle, Ditlev E. Brodersen, William M. Clemons Jr.,  
Michael J. Tarry, Andrew P. Carter, V. Ramakrishnan\*

Crystal structures of the 30S ribosomal subunit in complex with messenger RNA and cognate transfer RNA in the A site, both in the presence and absence of the antibiotic paromomycin, have been solved at between 3.1 and 3.3 angstroms resolution. Cognate transfer RNA (tRNA) binding induces global domain movements of the 30S subunit and changes in the conformation of the universally conserved and essential bases A1492, A1493, and G530 of 16S RNA. These bases interact intimately with the minor groove of the first two base pairs between the codon and anticodon, thus sensing Watson-Crick base-pairing geometry and discriminating against near-cognate tRNA. The third, or "wobble," position of the codon is free to accommodate certain noncanonical base pairs. By partially inducing these structural changes, paromomycin facilitates binding of near-cognate tRNAs.

During protein synthesis, the ribosome catalyzes the sequential addition of amino acids to a growing polypeptide chain, using mRNA as a template and aminoacylated tRNAs (aa-tRNAs) as substrates. Correct base pairing between the three bases of the codon on mRNA and those of the anticodon of the cognate aa-tRNA dictates the sequence of the polypeptide chain. Discrimination against noncognate tRNA, which generally has two or three mismatches in the base pairing, can be accounted for by the difference in the free energy of base pairing to the codon compared with cognate tRNA. For near-cognate tRNA, which usually involves a single mismatch, the free-energy difference in base pairing compared with cognate tRNA would predict an error rate that is one to two orders of magnitude higher than the actual error rate of protein synthesis (1), and it has long been recognized that the ribosome must improve the accuracy of protein synthesis by discriminating against near-cognate tRNAs (2). This discrimination involves the 30S subunit, which binds mRNA and the anticodon stem-loop (ASL) of tRNA.

At the beginning of the elongation cycle, which involves the addition of a new amino acid to a growing polypeptide chain, the aa-tRNA is presented to the ribosome as a ternary complex with elongation factor Tu (EF-Tu) and guanosine triphosphate (GTP). The selection of cognate tRNA is believed to occur in two stages—an initial recognition step and a proofreading step—that are separated by the irreversible hydrolysis of GTP by EF-Tu (3–6). In this scheme, the discrimination energy inherent in

codon-anticodon base pairing is exploited twice to achieve the necessary accuracy. Recent experiments suggest that the binding of cognate rather than near-cognate tRNA results in higher rates of both GTP hydrolysis by EF-Tu, and accommodation, a process in which the acceptor arm of the aa-tRNA swings into the peptidyl transferase site after its release from EF-Tu (7, 8). In both steps, the higher rate is proposed to be the result of structural changes in the ribosome induced by cognate tRNA. In the context of proofreading mechanisms alone, it is unclear whether additional structural discrimination by the ribosome, over that inherent in the energetics of codon-anticodon base pairing, is actually required in decoding. In an alternative view, it was proposed that the ribosome contributes to the specificity of decoding by recognizing the geometry of codon-anticodon base pairing (9, 10), probably by direct recognition of the sugar phosphate backbone (11). This is consistent with evidence that the ribosome can discriminate between cognate and near-cognate tRNA with very high accuracy in a single step under near-equilibrium conditions (12), so that the recognition and proofreading steps may be needed not only for accuracy as proposed earlier, but for the combination of high speed and accuracy required in protein synthesis.

The heart of decoding involves recognition of Watson-Crick base pairing between the codon on mRNA and the anticodon found in positions 34 to 36 of the ASL of tRNA. This base pairing results in a short double helix that we call the codon-anticodon helix. Data from chemical protection (13), cross-linking (14), and genetic analysis (15) suggest that the decoding site is a region around the ribosomal A site that includes helix 44, the 530 loop, and helix 34 of 16S RNA, which are now known from the high-resolution structure of the 30S subunit to

be close to one another (16, 17).

Recent work on decoding has focused on an internal loop of helix 44 containing two universally conserved bases, A1492 and A1493. These bases are chemically protected at their N1 positions when tRNA is bound in the A site of the 30S subunit (13), and were shown to be essential for viability in *Escherichia coli* and for A-site tRNA binding (18). This loop is also the binding site of the antibiotic paromomycin that reduces the fidelity of decoding (19–21). Nuclear magnetic resonance (NMR) structures of a fragment of RNA containing this internal loop showed that these bases were displaced into the minor groove of helix 44 in the presence of paromomycin (20, 22). A direct interaction of the N1 of these bases with the 2' OH of mRNA was inferred on the basis of biochemical experiments (18). Based on these data, it was suggested that the changes induced by the antibiotic mimic those induced by cognate tRNA, that the bases would interact via their minor-groove side with the minor groove of the codon-anticodon helix, and that they would sense the shape of the codon-anticodon helix during decoding (18, 20, 22). However, in the absence of a structure in the context of the whole 30S subunit, it was also possible to use existing data to propose an alternative and quite different model of the decoding site that involved interaction of the codon-anticodon helix with the major rather than minor groove of helix 44 (23).

A 7.8 Å resolution structure of the 70S ribosome in complex with mRNA and tRNA (24) showed that at that resolution, the conformation of the internal loop in helix 44 was similar to that in the paromomycin-bound NMR structure of the isolated fragment (20). However, A1492 and A1493 in this internal loop appeared too far from the codon-anticodon helix to interact with it directly (24), so their role and the general structural basis of decoding by the ribosome remained unclear.

More recently, the crystal structure of the 30S subunit complexed with paromomycin, streptomycin, and spectinomycin (21) showed that A1492 and A1493 are completely flipped out from their stacked position inside the internal loop rather than just displaced into the minor groove, as previously proposed (20). The displaced bases point into the A site in a position that would indeed allow direct monitoring of the minor groove of the codon-anticodon helix. On the basis of this structure, we suggested that during decoding, these bases would flip out even in the absence of paromomycin, in a way that would allow discrimination of cognate from near-cognate tRNA (21). However, this conformation would place the N1 of the adenines pointing toward tRNA, and hence unable to make the interactions with mRNA previously reported (18).

In this work, we directly examine the interactions of the 30S subunit with mRNA and an ASL of cognate tRNA bound in the A site by

MRC Laboratory of Molecular Biology, Hills Road, Cambridge CB2 2QH, UK.

\*To whom correspondence should be addressed. E-mail: ramak@mrc-lmb.cam.ac.uk

x-ray crystallography.

**Structure determination.** Recently, we showed that the A site in our crystal form is accessible by diffusion of macromolecules as large as initiation factor IF1 (25). On the basis of this result, a 17-nucleotide fragment corresponding to the ASL of tRNA<sup>Phe</sup> with a GAA anticodon, along with a U<sub>6</sub> hexanucleotide that would place a codon for phenylalanine in the A site, were soaked into crystals of the 30S subunit (26). Diffraction data to 3.1 to 3.3 Å resolution were collected from such crystals both in the absence and presence of paromomycin, as well as from crystals of the 30S subunit soaked in paromomycin alone (Table 1). Initial refinement was done with the native 30S subunit structure (Protein Data Bank entry 1FJF) (17) as a starting model, with the occupancies of the atoms for parts of the structure in the vicinity of A-site tRNA initially set to zero to avoid possible bias (26). Clear density for the A-site codon and tRNA ASL, and elements of the 30S subunit that had changed conformation such as A1492, A1493, and G530 was visible in difference Fourier electron density maps (Fig. 1A) for the complexes both in the absence and presence of paromomycin. These elements were subsequently built into the maps for each of the individual structures, and a final refinement was done with all atoms visible in the electron density, including metal ions. Statistics for the refinement are shown in Table 1. A  $\sigma_A$ -weighted  $2mF_o - DF_c$  map after refinement is shown in Fig. 1B.

**Overview of mRNA and tRNA in the A site.** The structure reveals details of mRNA and tRNA binding to the 30S subunit (Fig. 2). In our native 30S subunit structure, the 3' end of 16S RNA is folded back into the message binding cleft of the 30S subunit, and thus mimics mRNA in the P and E sites (21). The P site is also occupied by a stem-loop that mimics tRNA and comes from helix 6 of a neighboring molecule in the crystal. These features are also seen in all the complexes described below. Additionally, in the structures with the ASL and U<sub>6</sub> hexanucleotide, we can clearly see the three nucleotides from the A-site codon, and slightly less well-defined density for a fourth nucleotide 3' of the A site. The electron density for the mRNA between the P and A sites appears continuous despite the presence of a covalent break in the chain between the P- and A-site codons. As reported earlier at lower resolution (24), there is a distinct kink in the path of the mRNA between the A- and P-site codons. In addition, we can now see in detail how the ASL of cognate tRNA interacts with the A-site codon and the 30S subunit. The structure of the ASL, which does not contain any modified nucleosides, is very similar to that of isolated yeast phenylalanine tRNA (27, 28) or of *Thermus* phenylalanine tRNA complexed with aminoacyl synthetase (29). The contacts of the ASL to the 530 loop, helix 34, and helix 44 of the

ribosome arise solely from the anticodon loop.

**Recognition of cognate tRNA in the ribosome by an induced fit.** The binding of mRNA and cognate tRNA in the A site induces A1492 and A1493 to flip out of the internal loop of helix 44. This binding also causes the universally conserved base G530, which has been footprinted by A-site tRNA (13), to switch from the *syn* conformation present in the native structure to an *anti* conformation. In their new conformations, A1493 and A1492 interact, respectively, with the first and second base pairs of the codon-anticodon helix, whereas G530 interacts with both the second position of the anticodon and the third position of the codon. The result of these induced changes is that the first two base pairs of the codon-anticodon helix are closely monitored by the ribosome in a way that would be able to discriminate between Watson-Crick base pairing and mismatches, whereas the environment of the third, or "wobble," position appears to be suited for accommodating other base-pairing geometries (30, 31).

A1493 packs tightly in the minor groove of the first base pair of the codon-anticodon helix, so that there are hydrogen bonds between the 2' OH of the A1493 and the 2' OH of the first nucleotide of the codon, as well as between N1 of A1493 and the 2' OH of position 36 of the anticodon (Fig. 3a). Additionally, a hydrogen bond is evident from the 2' OH of A1493 to the O2 of the uracil in the codon. Although this bond involves the base, it is not sequence specific because the O2 of pyrimidines and the N3 of purines are hydrogen bond acceptors that occupy equivalent positions in the minor groove

of Watson-Crick base pairs (32). In the case of a GC or CG base pair at the first codon position, it would be possible to form an additional bond from the N3 of the A1493 to the N2 of the guanine.

A1492 and G530 together bind in and span the minor groove of the second base pair of the codon-anticodon helix (Fig. 3B), and their orientation relative to one another is stabilized in part by a hydrogen bond between their N1 positions. They make equivalent interactions with each strand of the codon-anticodon helix in that the 2' OH of the codon hydrogen bonds to the N3 and the 2' OH of A1492, whereas the 2' OH of tRNA hydrogen bonds to the N3 and 2' OH of G530. In addition, the N6 of A1492 is involved in hydrogen bonding to the 2' OH of the universally conserved C518, as well as to the highly conserved Ser<sup>50</sup> (*E. coli* Ser<sup>46</sup>) of the nearby protein S12. The loop of S12 containing this serine (Pro<sup>45</sup> to Ser<sup>50</sup>; *E. coli* residues 41 to 46) is the site of mutations that affect the fidelity of translation (33). As with the first base pair, the close fit of van der Waals surfaces and various interactions in the minor groove would be sensitive to whether the second base pair had Watson-Crick geometry or not.

Unlike the first two base pairs, the geometry of the third base pair between the codon and anticodon, which in our structure is a GU base pair, is not as closely monitored by the ribosome (Fig. 3C). The 2' OH of the codon makes a hydrogen bond with the O6 of G530, as well as an indirect metal-mediated interaction with the O2 of C518 and the main-chain carbonyl of Pro<sup>48</sup> (*E. coli* Pro<sup>44</sup>) of protein S12. In addition,

Table 1. Summary of crystallographic data.

Data set	U6/ASL	U6/ASL/ paromomycin	Paromomycin
<i>Data collection</i>			
Beamline	SBC 19ID	SBC 19ID	SBC 19ID
Resolution limit (Å)	3.31	3.11	3.31
Unit cell			
<i>a, b</i> (Å)	401.57	400.80	401.16
<i>c</i> (Å)	176.11	175.88	176.36
No. of observations	968,646	1,170,885	1,079,968
No. of unique reflections	206,478	240,896	207,340
<i>R</i> <sub>sym</sub> * (%)	12.2 (65.4)	11.7 (57.8)	16.0 (66.4)
Completeness* (%)	97.5 (93.6)	95.1 (92.7)	97.8 (98.0)
$\langle I \rangle / \langle \sigma_I \rangle$ *	10.9 (2.6)	11.9 (2.8)	10.8 (2.7)
<i>Refinement</i>			
Resolution range (Å)	316.23–3.31	316.23–3.11	316.23–3.31
Reflections excluded for cross-validation	5%	5%	5%
Number of nonhydrogen atoms	52,109	52,250	51,880
Proteins	19,178	19,178	19,237
RNA	32,809	32,904	32,486
Metals	122	126	115
<i>R</i> factor† (%)	23.1 (28.6)	23.2 (27.5)	22.9 (28.2)
$\sigma_A$ coordinate error‡	0.56 (0.64)	0.48 (0.51)	0.53 (0.61)
Deviations from ideality			
rms deviations in bond lengths (Å)	0.007	0.007	0.007
rms deviations in bond angles (°)	1.23	1.21	1.23

\*Values for the outermost resolution shell are given in parentheses. †Values in parentheses represent the free *R* factor. ‡Values in parentheses represent the cross-validated  $\sigma_A$  coordinate error.

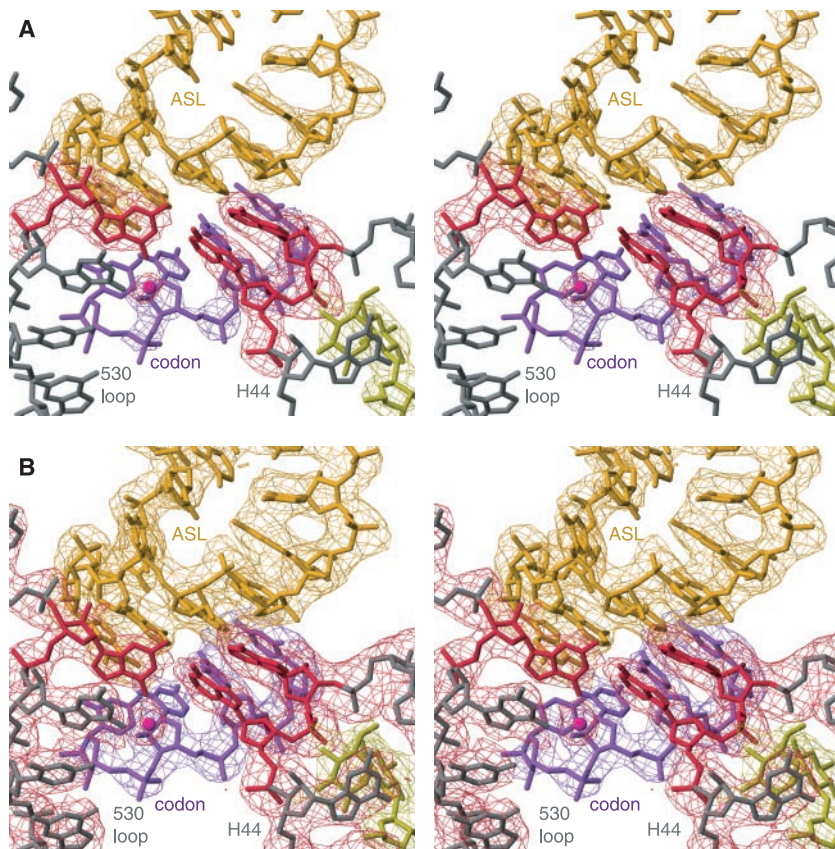


**Fig. 1.** Stereo views of the electron density for the 30S ribosomal subunit complex with mRNA and tRNA-ASL in the presence of paromomycin, around the site of the codon-anticodon interaction. Portions of the tRNA-ASL (gold), codon from a  $U_6$  hexanucleotide (purple), and 530 loop and helix 44 (gray), along with the bases G530 (red, left), A1492 and A1493 (red, right), and a  $Mg^{2+}$  ion (magenta sphere), are shown. Part of paromomycin is in yellow in the lower right. (A)  $mF_o - DF_c$  difference density based on a simulated annealing run, contoured at  $3\sigma$ . The tRNA-ASL,  $U_6$  hexanucleotide, paromomycin, and nucleotides 530 and 1492/3 were omitted from the refinement, and the density pertaining to each of these elements has been colored accordingly for clarity. (B) Refined  $2mF_o - DF_c$  electron density contoured at  $1.5\sigma$ . Figures 1, 2, and 4 were produced with O (51) and MOLMOL (52) and rendered with POV-Ray.

the pyrimidine O2 of the anticodon and the O6 of G530 are in close contact. The ribose of the anticodon packs against C1054 from helix 34 in the head of the ribosome. These interactions leave the minor groove of this base pair, especially on the anticodon side, relatively open as compared with the first two positions. Because noncanonical base pairs alter the shape and possible interactions in the minor groove, the structure shows why some of these are allowed in the wobble position. Also, the mRNA nucleotide in this position makes more interactions with the ribosome than does the tRNA, confirming predictions that its conformation should be the more restricted of the two (31).

The geometry of the first two base pairs of the codon-anticodon helix is very similar in the presence and absence of paromomycin, with a slightly less planar base pair in the first position in the presence of paromomycin. In the absence of paromomycin, the geometry for the third position deviates from that expected for a wobble pair (Fig. 3C), but the expected wobble geometry is seen in the higher resolution structure in the presence of paromomycin (Fig. 3D). Because we see occasional departures from ideality in other parts of the 30S subunit structure, higher resolution will be needed to make definitive statements about deviations from standard geometry.

The structure is consistent with most chemical protection (13) and genetic data (15) on A-site tRNA binding. The finding that A1492 and A1493 are required for viability (18) is rationalized by the observation that the smaller pyrimidines could not reach far enough to make interactions with tRNA or G530, and that guanine would not only have a steric clash at its N2 position, but would also not be able to hydrogen bond through its N1 in the same way. The

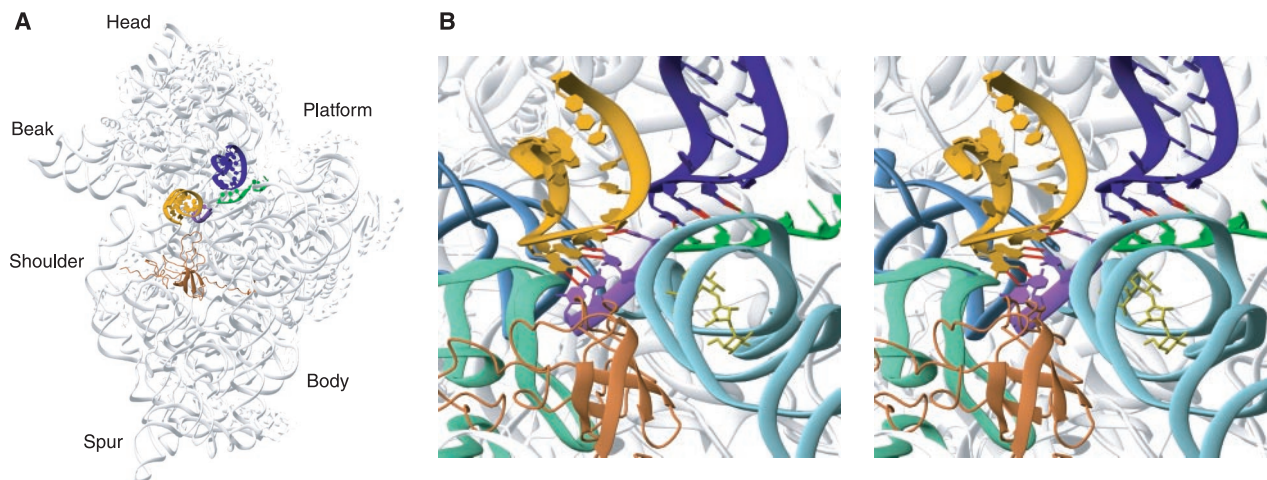


**Fig. 2.** Complex of the 30S subunit with mRNA from a  $U_6$  hexanucleotide and a cognate tRNA-ASL. (A) Overview of the complex. The 50S interface side of the 30S subunit is facing the reader, and important elements have been given standard colors that are used throughout the figures, namely, ASL at the A site (gold), codon from the  $U_6$  hexanucleotide at the A site (purple), 3' end of 16S RNA that mimics mRNA at the P site (green),

P site tRNA mimic introduced by helix 6 from a neighboring molecule (dark blue), and protein S12 (tan). (B) Stereo view showing details of the A and P sites, colored as in (A), with, in addition, helix 44 (cyan, right), helix 34 (blue, left), 530 loop (green, left), and paromomycin (yellow sticks, within helix 44). The hydrogen bonds responsible for the codon-anticodon interaction at both the A and P sites are shown as red lines.

requirement for guanine at position 530 (34) can be similarly rationalized, because its N1 is required to hydrogen bond with the N1 of A1492, and its O6 is required to hydrogen bond with the 2' OH of the uridine at the third position of the codon. Although A1492 and A1493 flip out of helix 44 and monitor the minor groove of the codon-anticodon helix roughly as we had proposed, the details of the interactions are different from those in the two motifs found in the structure of 16S RNA that we had suggested as

possible ways for adenines to recognize the codon-anticodon helix (21). Also, the N1 of these adenines interacts with the 2' OH of tRNA or with the N1 of G530, rather than with the 2' OH groups of mRNA, as proposed previously (18). Finally, the structure does not support a model in which the N6 of these adenines forms a hydrogen bond with the O2 of pyrimidines or N3 of purines on mRNA (23).

Both the structural interactions and the

general strategy in decoding have similarities with other systems. The interactions that A1493 and A1492 make with the minor groove of the first two base pairs of the codon-anticodon helix are identical to tertiary interactions that occur in both the group I intron (35) and the structure of 23S RNA (36), and are classified as consecutive "Type I" and "Type II" A-minor motif interactions (37). These interactions always involve conserved adenines, and a major part of the stabilization energy arises from the complementarity of the adenines with the surface of the minor groove (38). Similar tertiary interactions involving tight packing of conserved adenines in minor grooves of adjacent helices have also been reported in the 16S RNA structure (17, 21).

The strategy adopted by the ribosome to recognize correct base pairing has similarities and differences with other template-directed enzymes that have high fidelity such as DNA and RNA polymerases. These enzymes also make close interactions with the minor groove of the base pair to be formed. In DNA polymerases, conserved arginines or glutamines form hydrogen bonds to the O2 of pyrimidines or N3 of purines (39, 40). In our structures, A1493 does make a similar hydrogen bond with the O2 of uracil in monitoring the first codon base. However, the ribosome mainly forms bonds with the ribose 2' OH groups on both strands of the codon-anticodon helix, which are not available to DNA polymerases. Interestingly, T7 RNA polymerase also forms hydrogen bonds to 2' OH moieties of the incoming ribonucleotide and the RNA transcript (41). It is clear that the ribosome, like polymerases, senses the shape and available interactions at the minor groove to ensure fidelity.

**Effect of paromomycin.** The effects of tRNA and paromomycin on the 30S subunit are shown schematically in Fig. 4. In the native structure (17), A1492 and A1493 are stacked in the interior of helix 44 (Fig. 4A), and G530 is stacked in the 530 loop in the *syn* conformation. The binding of paromomycin flips out A1492 and A1493 (Fig. 4B). The structure of the decoding site in the presence of paromomycin alone is essentially identical to that determined previously in the presence of paromomycin, streptomycin, and spectinomycin (21), showing that the changes induced in this region are solely due to the binding of paromomycin. However, in the absence of tRNA, paromomycin does not have an effect on G530, which remains in the *syn* conformation. The binding of A-site tRNA flips out G530 into the *anti* conformation (Fig. 4C); it also flips out A1492 and A1493, but they are not in exactly the same conformation as with paromomycin alone (compare Fig. 4, B and C). In the presence of cognate A-site tRNA, the additional presence of

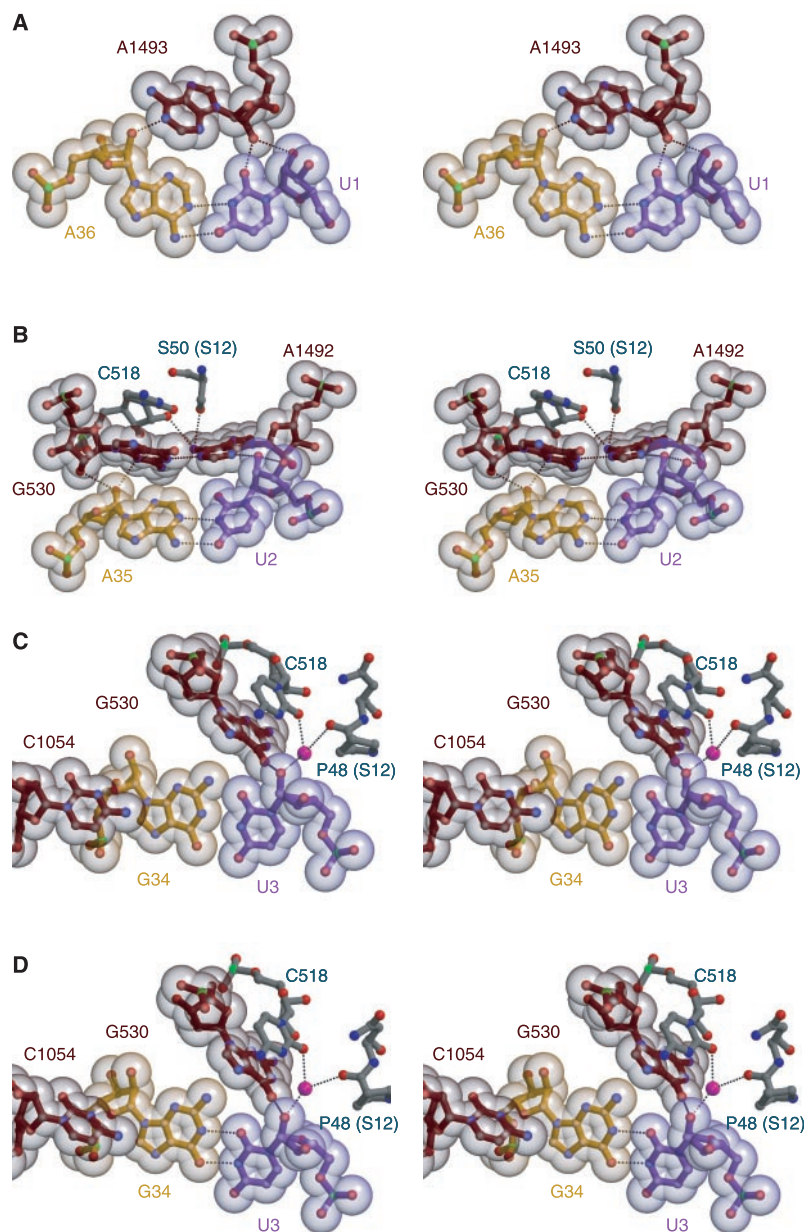


**Fig. 3.** Stereo views showing interactions of the ribosome with the codon-anticodon base pairs. The tightness of the interactions is shown by the semitransparent van der Waals surface. (A) In the first position, A1493 binds in the minor groove of the A36-U1 base pair. (B) In the second position, G530 and A1492 (both brown) act in concert to monitor the A35-U2 base pair. (C) The third (wobble) position, showing the G34-U3 base pair. C1054 stacks against G36 of the ASL. U3 interacts with G530, and indirectly through a  $Mg^{2+}$  ion (magenta) with C518 and residue Pro<sup>48</sup> (*E. coli* Pro<sup>44</sup>) from protein S12 (gray). The base pair seems closer to Watson-Crick geometry. (D) The third position in the presence of paromomycin, with the expected GU wobble pair. The interactions with the ribosome are similar to those in (C).

paromomycin (Fig. 4D) does not result in further changes in the conformation of these bases (compare Fig. 4, C and D).

The structures provide firm evidence that the changes induced in the 30S subunit by cognate tRNA are energetically favorable because various compensating interactions can be made by the ribosome with the codon-anticodon helix, but only when the first two base pairs are canonical Watson-Crick base pairs. In the case of near-cognate tRNA, fewer of these interactions would be possible, so the induced changes would normally be less favorable. By paying part of the energetic cost of these induced changes, especially in displacing A1492 and A1493 from their internal loop in helix 44, paromomycin facilitates the binding of near-cognate tRNAs, along with the full changes induced as a result. This model is consistent with the finding that paromomycin accelerates precisely those steps (GTP hydrolysis and accommodation) for near-cognate tRNA that are normally slower as compared with cognate tRNA (8) and agrees with earlier proposals that paromomycin works by inducing structural changes in the decoding site (21, 22), rather than by making direct interactions with mRNA or tRNA (23). The structure also explains the classical result that single-stranded DNA is not normally a good template for protein synthesis, but becomes so in the presence of the antibiotics neomycin and kanamycin, which are closely related to paromomycin (42). Because the 2' OH groups are not present on DNA, the induced structural changes on cognate tRNA binding are not normally favorable because fewer interactions are possible. However, just as with normal translation, aminoglycosides can pay for part of the energetic cost of the induced changes and stabilize tRNA binding.

**Other conformational changes during decoding.** During accommodation, the A-site tRNA has to rotate significantly from its initial orientation as part of the ternary complex with EF-Tu to its final position in the A site, where its acceptor end is accessible to peptidyl transferase (43, 44). From an examination of the A-site tRNA in 70S ribosome structures (24, 45, 46), it appears that the position of the ASL in our structure is close to the tRNA orientation after accommodation. Because most of the selectivity of cognate over near-cognate tRNA appears to come from the accommodation step (7), the structure we see is likely to be relevant for understanding the specificity of the ribosome for cognate tRNA. A high-resolution structure of the EF-Tu ternary complex bound to the ribosome will be required to understand details of the initial recognition step. However, it is likely that many of the changes induced by cognate tRNA are initiated during the binding of the ternary complex, and that the resulting interactions of the ribosome with the codon-anticodon helix persist during the subsequent movement of the tRNA.

A key question that remains to be answered is how the changes around the decoding site induced by cognate tRNA are transmitted to EF-Tu to trigger GTP hydrolysis. The binding of cognate tRNA results in a movement of the head and shoulder of the 30S subunit toward each other so that they close around the A-site tRNA. These changes are even greater when paromomycin is bound in addition to cognate tRNA, with as much as a 4 Å relative movement between the head and shoulder [see supplementary information (47)]. As with the binding of IF1 (25), it is likely that we do not see the full extent of conformational changes because of the constraints of the crystal lattice. It is possible that these changes reflect the types of changes in the 30S subunit that occur on the binding of the EF-Tu ternary complex, which may be transmitted to the 50S subunit and be part of the trigger for GTP hydrolysis by EF-Tu. Another possibility, suggested on the basis of

experiments in which the acceptor arm and the ASL of cognate tRNA were present as two separate fragments, is that the signal to EF-Tu is transmitted through tRNA itself (48).

**Conclusions.** This work shows that the ribosome recognizes the geometry of codon-anticodon base pairing in a way that would discriminate against near-cognate tRNAs. The minor groove of the first and second base pairs between the codon and anticodon is closely monitored by a set of interactions that are induced by the binding of cognate tRNA. These interactions would be disrupted by mismatches, so that the induced structural changes would no longer be energetically favorable. The third or “wobble” position has less stringent constraints, and therefore can allow a broader range of base-pairing geometries, consistent with the requirements of the genetic code. The binding of paromomycin partially induces the changes that normally are induced by cognate tRNA. By

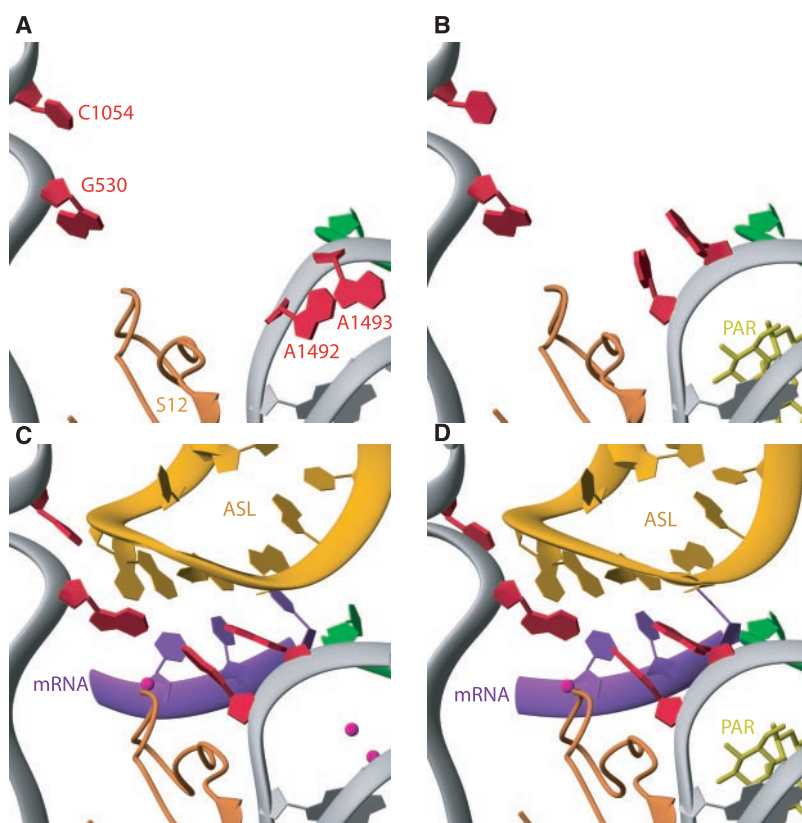


**Fig. 4.** Discrete states of the A site of the 30S subunit, as deduced from four different crystal structures. In all panels, the tRNA ASL (gold), A-site mRNA codon (purple), P-site mRNA (green), protein S12 (brown), and important bases (red) involved in conformational changes are shown. A few elements of the 16S RNA such as helix 44 (lower right), 530 loop (mid and lower left), and helix 34 (upper left) are also shown. (A) The native 30S subunit (17). A1492 and A1493 (red, right) are stacked in the interior of H44, and G530 is in the *syn* conformation. C1054 is shown in the upper left corner. (B) In the presence of paromomycin, the bases of A1492 and A1493 have been displaced into the A site by the binding of the antibiotic inside helix 44 (lower right), 530 loop (mid and lower left), and helix 34 (upper left) are also shown. (C) When the codon and cognate tRNA-ASL bind in the A site, A1492 and A1493 flip out to monitor the codon-anticodon interaction, and G530 has switched to the *anti* conformation to interact with A1492, the anticodon in the second position, and the codon in the third. Two  $Mg^{2+}$  ions (magenta spheres) are visible near the region vacated by A1492 and A1493 in the interior of helix 44, and one is located close to the ribose of the codon in the wobble position (see Fig. 3, C and D). (D) When paromomycin is present in addition to tRNA-ASL and codon, the structure is very similar to that in (C).

paying part of the energetic cost of these induced changes, paromomycin facilitates the increased incorporation of amino acids from near-cognate tRNAs.

## References and Notes

- Reviewed in M. Ibbá, D. Söll, *Science* **286**, 1893 (1999).
- J. Davies, W. Gilbert, L. Gorini, *Proc. Natl. Acad. Sci. U.S.A.* **51**, 883 (1964).
- J. J. Hopfield, *Proc. Natl. Acad. Sci. U.S.A.* **71**, 4135 (1974).
- J. Ninio, *Biochimie* **57**, 587 (1975).
- R. C. Thompson, P. J. Stone, *Proc. Natl. Acad. Sci. U.S.A.* **74**, 198 (1977).
- T. Ruusala, M. Ehrenberg, C. G. Kurland, *EMBO J.* **1**, 741 (1982).
- T. Pape, W. Wintermeyer, M. Rodnina, *EMBO J.* **18**, 3800 (1999).
- , *Nature Struct. Biol.* **7**, 104 (2000).
- M. Eigen, L. De Maeyer, *Naturwissenschaften* **53**, 50 (1966).
- A. P. Potapov, *FEBS Lett.* **146**, 5 (1982).
- , F. J. Triana-Alonso, K. H. Nierhaus, *J. Biol. Chem.* **270**, 17680 (1995).
- R. C. Thompson, A. M. Karim, *Proc. Natl. Acad. Sci. U.S.A.* **79**, 4922 (1982).
- D. Moazed, H. F. Noller, *J. Mol. Biol.* **211**, 135 (1990).
- F. Mueller, H. Stark, M. van Heel, J. Rinke-Appel, R. Brimacombe, *J. Mol. Biol.* **271**, 566 (1997).
- M. O'Connor et al., *Biochem. Cell Biol.* **73**, 859 (1995).
- F. Schluenzen et al., *Cell* **102**, 615 (2000).
- B. T. Wimberly et al., *Nature* **407**, 327 (2000).
- S. Yoshizawa, D. Fourmy, J. D. Puglisi, *Science* **285**, 1722 (1999).
- D. Moazed, H. F. Noller, *Nature* **327**, 389 (1987).
- D. Fourmy, M. I. Recht, S. C. Blanchard, J. D. Puglisi, *Science* **274**, 1367 (1996).
- A. P. Carter et al., *Nature* **407**, 340 (2000).
- D. Fourmy, S. Yoshizawa, J. D. Puglisi, *J. Mol. Biol.* **277**, 333 (1998).
- M. S. VanLoock, T. R. Easterwood, S. C. Harvey, *J. Mol. Biol.* **285**, 2069 (1999).
- J. H. Cate, M. M. Yusupov, G. Z. Yusupova, T. N. Earnest, H. F. Noller, *Science* **285**, 2095 (1999).
- A. P. Carter et al., *Science* **291**, 498 (2001).
- Crystals of the 30S subunit from *T. thermophilus* were grown as described (17). A tRNA<sup>Phe</sup> ASL corresponding to the sequence GGGGAUUGAAAUCGCC, and the U<sub>6</sub> hexanucleotide were synthesized chemically. The ASL and U<sub>6</sub> hexanucleotide were purified by gel electrophoresis. Crystals were transferred to a stabilizing buffer containing 26% 2-methyl-2,4-pentanediol (MPD) as described (17). Soaks of equimolar ASL and U<sub>6</sub> were done at a concentration of 100 or 300 μM in the same stabilizing buffer, while paromomycin, if present, was at a concentration of 80 μM. Initial screening of crystals was done at beamlines 14.1 and 14.2 at the Synchrotron Radiation Source at Daresbury Laboratory (Warrington, UK), where a 3.8 Å resolution data set on one of the soaks was also collected. All data to high resolution were collected at beamline SBC-19ID at the Advanced Photon Source at Argonne National Laboratory (Illinois), integrated and scaled with HKL-2000 (49). The atomic structure of the 30S subunit (17), omitting various parts near the A site, was used as a starting point for refinement against the three data sets with CNS (50). Initially, rigid-body refinement was done with the domains of 16S RNA and the individual proteins as separate rigid objects. This was followed by positional refinement, simulated annealing with torsion angle dynamics, and then two rounds of grouped B-factor refinement and refinement of the occupancies of metal ions. The ASL (15 and 11 residues in the presence and absence of paromomycin, respectively), mRNA, and any changes in the 30S subunit were built into the density in difference Fourier maps with the program O (51) before a final round of refinement. Coordinates have been deposited in the Protein Data Bank with accession numbers 1IBK (30S/paromomycin), 1IBL (30S/ASL/U<sub>6</sub>/paromomycin), and 1IBM (30S/ASL/U<sub>6</sub>). Coordinates of individual components will be made available on <http://alf1.mrc-lmb.cam.ac.uk/~ramak/30S>.
- H. Shi, P. B. Moore, *RNA* **6**, 1091 (2000).
- L. Jovine, S. Djordjevic, D. Rhodes, *J. Mol. Biol.* **301**, 401 (2000).
- Y. Goldgur et al., *Structure* **5**, 59 (1997).
- F. H. C. Crick, *J. Mol. Biol.* **19**, 548 (1966).
- S. Yokoyama, S. Nishimura, in *tRNA: Structure, Biosynthesis and Function*, D. Söll, U. Rajbhandary, Eds. (American Society for Microbiology, Washington, DC, 1995), pp. 207–223.
- N. C. Seeman, J. M. Rosenberg, A. Rich, *Proc. Natl. Acad. Sci. U.S.A.* **73**, 804 (1976).
- Reviewed in C. G. Kurland, D. Hughes, M. Ehrenberg, in *Escherichia coli and Salmonella typhimurium*; *Cellular and Molecular Biology*, F. C. Neidhardt et al., Eds. (American Society for Microbiology, Washington, DC, ed. 2, 1996), vol. 1, pp. 979–1004.
- T. Powers, H. F. Noller, *Proc. Natl. Acad. Sci. U.S.A.* **87**, 1042 (1990).
- J. Cate et al., *Science* **273**, 1696 (1996).
- N. Ban, P. Nissen, J. Hansen, P. B. Moore, T. A. Steitz, *Science* **289**, 905 (2000).
- P. Nissen, J. Ippolito, N. Ban, P. B. Moore, T. A. Steitz, *Proc. Natl. Acad. Sci. U.S.A.* (online), 10 April 2001.
- E. A. Doherty, R. T. Batey, B. Masquida, J. A. Doudna, *Nature Struct. Biol.* **8**, 339 (2001).
- S. Double, S. Tabor, A. M. Long, C. C. Richardson, T. Ellenberger, *Nature* **391**, 251 (1998).
- J. R. Kiefer, C. Mao, J. C. Braman, L. S. Beese, *Nature* **391**, 304 (1998).
- G. M. Cheetham, T. A. Steitz, *Science* **286**, 2305 (1999).
- B. J. McCarthy, J. J. Holland, *Proc. Natl. Acad. Sci. U.S.A.* **54**, 880 (1965).
- H. Stark et al., *Nature* **389**, 403 (1997).
- R. K. Agrawal et al., *J. Cell Biol.* **150**, 447 (2000).
- R. K. Agrawal et al., *Science* **271**, 1000 (1996).
- H. Stark et al., *Cell* **88**, 19 (1997).
- Supplementary data are available on Science Online at [www.sciencemag.org/cgi/content/full/292/5518/897/DC1](http://www.sciencemag.org/cgi/content/full/292/5518/897/DC1).
- O. Piepenburg et al., *Biochemistry* **39**, 1734 (2000).
- Z. Otwinowski, W. Minor, in *Methods in Enzymology*, C. W. J. Carter, R. M. Sweet, Eds. (Academic Press, New York, 1997), vol. 276, pp. 307–325.
- A. T. Brünger et al., *Acta Crystallogr. D Biol. Crystallogr.* **54**, 905 (1998).
- T. A. Jones, M. Kjeldgaard, *Methods Enzymol.* **277B**, 173 (1997).
- R. Koradi, M. Billeter, K. Wüthrich, *J. Mol. Graphics* **14**, 51 (1996).
- We thank S. Ginell and A. Joachimiak (APS) and M. MacDonald and E. Duke (Daresbury) for their help and advice with synchrotron data collection; P. Nissen for comments on making Fig. 3; and B. T. Wimberly and K. Nagai for comments on the manuscript. Supported by the Medical Research Council (U.K.) and grant GM 44973 from the NIH to S. W. White and V.R. D.E.B. was the recipient of a Human Frontier Science Program postdoctoral fellowship.

12 March 2001; accepted 3 April 2001

## REPORTS

## Feynman's Path-Integral Approach for Intense-Laser-Atom Interactions

P. Salières,<sup>1</sup> B. Carré,<sup>1</sup> L. Le Déroff,<sup>1</sup> F. Grasbon,<sup>2</sup> G. G. Paulus,<sup>2</sup> H. Walther,<sup>2</sup> R. Kopold,<sup>3</sup> W. Becker,<sup>3</sup> D. B. Milošević,<sup>4</sup> A. Sanpera,<sup>5</sup> M. Lewenstein<sup>5\*</sup>

Atoms interacting with intense laser fields can emit electrons and photons of very high energies. An intuitive and quantitative explanation of these highly nonlinear processes can be found in terms of a generalization of classical Newtonian particle trajectories, the so-called quantum orbits. Very few quantum orbits are necessary to reproduce the experimental results. These orbits are clearly identified, thus opening the way for an efficient control as well as previously unknown applications of these processes.

Quantum mechanics has been successful in explaining the physics of the microworld. Its standard mathematical formulation, which provides the basis for calculations of

quantum-mechanical processes (1), requires a nearly complete break with classical intuition. In contrast, the alternative formulation of quantum mechanics devel-

oped by Feynman in terms of path integrals builds on the familiar Lagrangian concept of the action of an orbit in space and time and appears to be much closer to classical concepts (2). In Feynman's formulation, the probability amplitude of any quantum-mechanical process can be represented as a coherent superposition of contributions of all possible spatio-temporal paths that connect the initial and the final state of the system. The weight of each path is a complex number whose phase is equal to the classical action along the path. Even though this approach turned out to be very useful

<sup>1</sup>Centre d'Etudes de Saclay, CEA/DRECAM/SPAM, 91191 Gif-sur-Yvette, France. <sup>2</sup>Max-Planck-Institut für Quantenoptik, 85748 Garching, Germany. <sup>3</sup>Max-Born-Institut, 12489 Berlin, Germany. <sup>4</sup>Faculty of Science, University of Sarajevo, 71000 Sarajevo, Bosnia and Hercegovina. <sup>5</sup>Institute for Theoretical Physics, Universität Hannover, 30167 Hannover, Germany.

\*To whom correspondence should be addressed. E-mail: [lewen@itp.uni-hannover.de](mailto:lewen@itp.uni-hannover.de)